Chinese Chemical Letters 37 (2026) 112040

Contents lists available at ScienceDirect

Chinese Chemical Letters

journal homepage: www.elsevier.com/locate/cclet

Slow photons effect amplifying photo/photothermocatalytic solar fuel production

Yang Ding[a,*], Shuzeng Zhang[a], Zhixue Li[a], Guoxiang Yang[b,*], Runtian Zheng[c], Ning Han[d], Chunhua Wang[e,*]

[a] College of Materials and Environmental Engineering, Hangzhou Dianzi University, Hangzhou 310018, China
[b] School of Environmental Science and Engineering, Zhejiang Gongshang University, Hangzhou 310018, China
[c] Laboratory of Inorganic Materials Chemistry (CMI), University of Namur, Namur B-5000, Belgium
[d] Department of Electrical and Computer Engineering, University of Toronto, Toronto, ON M5S 3G4, Canada
[e] Department of Electrical Engineering and Computer Science, University of Michigan, MI 48109, United States

ARTICLE INFO

Article history:
Received 12 June 2025
Revised 22 October 2025
Accepted 30 October 2025
Available online 30 October 2025

Keywords:
Slow photon effect
Photonic crystal
CO_2 conversion
Water splitting
Solar fuel production

ABSTRACT

Transforming sunlight into renewable energy sources like hydrogen and methane through photocatalytic water splitting and the CO_2 conversion presents a promising prospect to tackle energy scarcity and environmental pollution caused by burning fossil fuels. As the core of the photocatalytic technique, photocatalysts design is most significant for acquiring the desirable catalytic performance and target products. Photonic crystals, also denoted as inverse opals and three-dimensionally ordered macroporous materials (3DOM), have been extensively applied in photocatalytic fields due to their distinct advantages. Specifically, photonic crystal possesses slow photons effect, rich reactive sites, and well-interconnected inner channels. Among the above advantages, the slow photons effect contributes the most essential role for accelerating photocatalytic reaction. However, how to design materials with maximized slow photons effect upon specific wavelength illumination is still in the infancy. Although some reviews about 3DOM photocatalysts have been published, a critical review focusing on tunable slow photons effects for efficient photocatalysis is still lacking. In this review, we highlighted recent advances in slow photons effect in boosting solar energy conversion. Meanwhile, the relevant mechanism and fundamentals of the slow photons effect are discussed. Finally, we present our vision of the future developments and challenges in this exciting research field.

© 2025 Published by Elsevier B.V. on behalf of Chinese Chemical Society and Institute of Materia Medica, Chinese Academy of Medical Sciences.

1. Introduction

In the past few decades, the fast developments of economy, science and industry have resulted in the tremendous consumption of fossil fuels including coal, oil, and natural gas, bringing out great issues of environmental pollution and energy shortage [1–5]. Since the groundbreaking work in terms of sunlight-driven H_2O splitting was carried out by Fujishima and co-workers in 1972 [6], using photocatalysis technique to convert solar energy into chemical energy has been widely studied in various reactions, such as pollutants decomposition, H_2/O_2 evolution, N_2 fixation, inorganic conversion and H_2O_2 synthesis [7–12]. Meanwhile, a variety of semiconductor photocatalysts (such as metal oxides, metal sulfides, and nitride) with different micro/nano structure have been exploited as advanced photocatalysts for various photocatalytic reactions [13–16]. As to photocatalysis process, the active photocatalyst materials are highly essential to make sure the photoinduced charges into a higher energy level to trigger photoredox reactions [17–20]. Light absorption, photoinduced hole-electron pair separation, surface charge migration and product desorption are involved in the whole photocatalysis system [21–25]. So far, various strategies have been developed to improve the photocatalytic efficiency, nevertheless, how to effectively utilize sun light *via* the slow photons effect has been always ignored in photocatalyst material design.

As to some materials with periodic structures (such as inverse opal), the light speed would be reduced as the irradiation light passes the material, which is also called as slow photon effect. Slow photon effect can enhance the residence time and absorption capability of irradiation light energy, improving the interaction between light and materials (Fig. 1a) [26–28]. In fact, the variable colors of butterfly wings, peacock feathers, beetle shells, and so on in nature often originates from the selective reflection and

* Corresponding authors.
E-mail addresses: dingyang@hdu.edu.cn (Y. Ding), yangguoxiang@zjgsu.edu.cn (G. Yang), chunhuaw@umich.edu (C. Wang).

https://doi.org/10.1016/j.cclet.2025.112040
1001-8417/© 2025 Published by Elsevier B.V. on behalf of Chinese Chemical Society and Institute of Materia Medica, Chinese Academy of Medical Sciences.

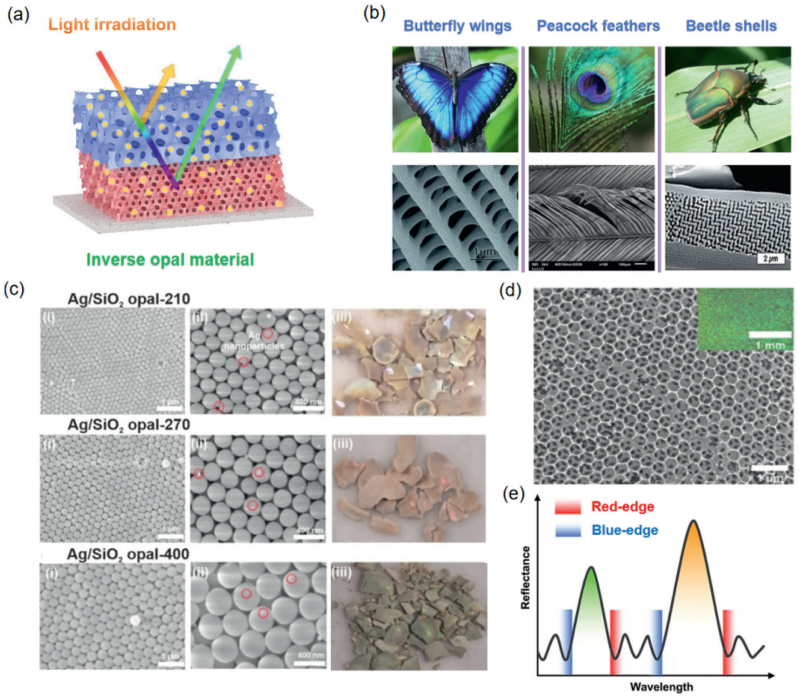


Fig. 1. (a) The slow photon effect on inverse opal structured materials. (b) The organisms with different color (top) and SEM images of their periodic nanostructures (bottom). (c) SEM images of the synthesized SiO_2 photonic crystal with different sizes (left) and colors of photographs (right). Reproduced with permission [9]. Copyright 2024, Wiley-VCH. (d) SEM image of the prepared inverse opal TiO_2 sample and photograph with green color (inset). (e) The red-edge and blue-edge of the reflectance spectra of inverse opal. Reproduced with permission [11]. Copyright 2023, Elsevier.

absorption of specific wavelengths by the periodic nanostructures of photonic crystals (Fig. 1b) [24], which often involve slow photons effect. Photonic crystal is a material with a periodic dielectric structure, which can precisely control the propagation of light in the same way that semiconductors control electrons. The most important characteristic of photonic crystals is the photonic bandgap. Inspired by the photonic crystal structures in nature, a series of artificially synthesized photonic crystal materials (such as SiO_2) have been reported (Fig. 1c) [9], which can improve the absorption of light with specific wavelengths and exhibit variable color *via* tuning the size of nanosphere. Typically, the inverse opal TiO_2 sample with pore size around 330 nm exhibits green color (Fig. 1d) under daylight [11]. The spectrum formed by the reflection of incident light *via* the photonic bandgap suggests that there are two boundaries for the reflection peak corresponding to a specific photonic bandgap. The boundary of the reflection peak that corresponds to longer wavelengths and lower energy is referred to as the red-edge, whereas the boundary associated with shorter wavelengths and higher energy is called the blue-edge (Fig. 1e) [11]. Theoretical analyses have shown that during the red-edge slow photon effect, incoming photons travel through the photonic crystal structured materials, while in the case of the blue-edge slow photon effect, the photons are situated within the pore structure of the 3DOM configuration [29,30]. When the energy of slow photons matches well with the bandgap width of the semiconductor photocatalyst, slow photons will be utilized by the photocatalyst and the light absorption efficiency will be greatly improved, thus improving photocatalytic performance.

As a type of nanomaterial with unique pore structure, photonic crystals, also denoted as three-dimensionally ordered macroporous (3DOM) materials, have been widely studied in catalytic fields [31–35]. The periodic internal pore channels can bring out the multiple light scattering and lead to slow photons effect so as to boost the photocatalytic procedure (Fig. 2a) [36]. Moreover, their high specific surface area can offer sufficient reactive sites for reactant adsorption and activation in different photocatalytic reactions (Fig. 2b) [37–40]. Thus, the photonic crystal structured materials endow great prospects in sustainable energy production alleviate current energy crisis. In this review, we firstly introduced the fundamentals and mechanisms of solar light induced catalytic energy conversion *via* slow photon effects. Then, the design strategies for inverse opal structured materials aimed at enhancing photocatalysis were outlined, emphasizing the advantages of these nanostructured catalysts in terms of reactive sites, mass diffusion, light absorption, and local photothermal effects, among other factors. Subsequently, the discussion then delves into the recent advancements in photocatalytic water splitting for hydrogen production, as well as the generation of clean fuels and valuable chemicals through photo/photothermal catalytic CO_2 conversion using inverse opal structured catalysts. Finally, the perspectives and challenges of solar light-driven sustainable energy conversion over photonic crystal catalysts are outlooked and elaborated. We sincerely hope that this important review will inspire innovative ideas for developing effective nanostructured photocatalysts and enhance our understanding of the solar energy conversion process, ultimately helping to reach the objectives of carbon peak and carbon neutrality.

2. Basics and mechanisms of photocatalytic solar fuel generation

Photocatalysis is a technology that harnesses light energy to facilitate chemical reactions. It primarily involves several essential steps: absorbing light, generating photoinduced charge carriers, separating electron-hole pairs, moving the photogenerated electrons and holes, and conducting surface photoredox reactions [41–43]. Photogenerated electrons typically undergo reduction reactions with the adsorbed oxidants (such as oxygen molecules, protons, CO_2) [44,45], while holes undergo oxidation reactions with reducing agents (such as water molecules or organic substances) [46,47]. The series of oxidation–reduction reactions triggered by

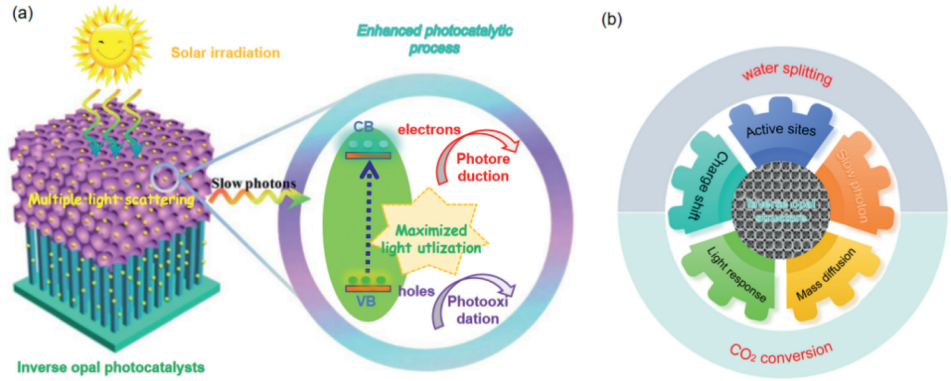


Fig. 2. (a) The scheme of inverse opal structured photocatalysts for efficient photocatalysis *via* slow photons effect. (b) The advantages of inverse opal structured materials for photocatalytic reactions.

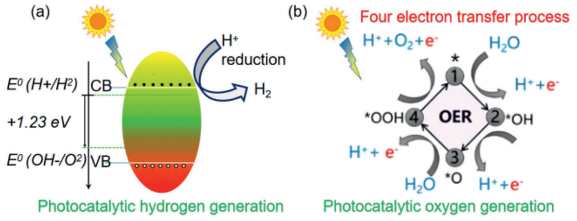


Fig. 3. (a) The schematic process of solar light driven photocatalytic water decomposition for hydrogen generation and (b) oxygen evolution *via* four electron transfer process.

photogenerated electrons and holes are the core of the photocatalytic process [48–50]. Photocatalytic technology has been utilized in various areas for clean and sustainable energy conversion, including hydrogen production through water splitting and the generation of fuels and valuable chemicals from CO_2 conversion. This technology enables the easy production of green energy and offers innovative ideas and opportunities for future energy transformation systems.

2.1. Photocatalytic hydrogen/oxygen production

To conduct photocatalytic water decomposition to release hydrogen and oxygen, the CB potential of semiconductor photocatalyst materials should be slightly negative than the hydrogen reduction potential H^+/H_2, while the VB potential should be positive than the oxygen oxidation potential O_2/H_2O (Fig. 3a) [51–54]. When exposed to external light, if the energy of the incoming photons is equal to or exceeds the bandgap of a semiconductor, electrons can be excited from the valence band (VB) to the conduction band (CB). Meanwhile, holes stay in the VB of the semiconductor. This process leads to the separation of electrons and holes, which can then facilitate the reduction of water to create hydrogen gas or the oxidation of water to generate oxygen gas at various sites within the semiconductor photocatalysts [55]. In comparison to the hydrogen evolution from water splitting, the oxygen formation half reaction in photocatalytic water splitting is a more difficult step as it involves a four-electron transfer process (Fig. 3b). The co-catalysts were frequently adopted for photocatalytic oxygen evolution *via* water splitting [56]. The most active oxygen evolution reaction co-catalysts are precious metal oxides (RuO_2 and IrO_2) [57]. But the interface formed between semiconductors and co-catalysts affects charge separation and transfer [58]. How to regulate the interface to accelerate hole transport and achieve efficient oxygen production efficiency is a great challenge. Up to now, a variety of semiconductor materials including CdS, TiO_2, C_3N_4 and Bi based photocatalysts have been explored for photocatalytic water decomposition. However, how to maximumly utilize solar/visible light by these semiconductor photocatalysts for efficient hydrogen/oxygen production is still highly difficult. Designing photocatalyst with inverse opal structure can improve light harvesting ability owing to slow photon effect, thus accelerating photocatalytic water splitting.

2.2. Photocatalytic/photothermal catalytic CO_2 conversion

As to the CO_2 conversion, it is necessary to provide enough energy to broke the two linear double bonds (C=O) due to the thermal stable and chemically inert properties of CO_2 molecule [59–61]. In early stage, thermocatalysis approach for CO_2 conversion has been extensively studied. In the process of thermocatalytic CO_2 reduction, the input of thermal energy and the presentation of catalysts are prerequisites for activating CO_2 molecules [62]. In particular, the C=O bonds are split and subsequent generation of new bonds upon high-energy environments. The total thermocatalytic CO_2 reduction is commonly composed of following steps: CO_2 molecule adsorption and activation, intermediates evolution, and the generation and desorption of products. Among the above procedures, intermediates production is widely considered as the rate-determining program of the total progress, being closely dependent on the surface chemistry of the thermocatalyst materials. Moreover, the fast desorption of the products from the catalyst surface is also essential, which would decide the cycle stability of the thermocatalytic CO_2 conversion system [63]. Different from the thermocatalytic reaction, the irradiated light as driven force is adopted to initiate photocatalytic CO_2 reduction (Fig. 4a) [64–66]. In this case, semiconductor materials as photocatalysts are frequently utilized because their appropriate electronic band gap structures can effectively excited by ultraviolet (UV) or visible light. Once the semiconductor photocatalysts are excited, the photoinduced electrons and holes can be produced on the CB and VB of the photocatalysts. The photogenerated charges can directly shift to the photocatalyst surface to activate or combine the CO_2 molecules, followed by the generation of intermediate species to achieve the conversion of CO_2 (Fig. 4b) [67]. The main gas products of photocatalytic CO_2 reduction reaction are CO and CH_4, may accompanied by the decomposition of water to produce hydrogen and oxygen, and may also produce alkane and alkene products [68]. Therefore, in addition to improve the photocatalytic CO_2 reduction rate, the selectivity modulation of the products from CO_2 reduction is also important for the practical application [69,70]. In addition to thermocatalysis and photocatalysis, photothermal catalysis has recently emerged as a very promising method for CO_2 reduction. This approach takes advantage of the wide absorption of solar energy to enhance both thermochemical and photochemical

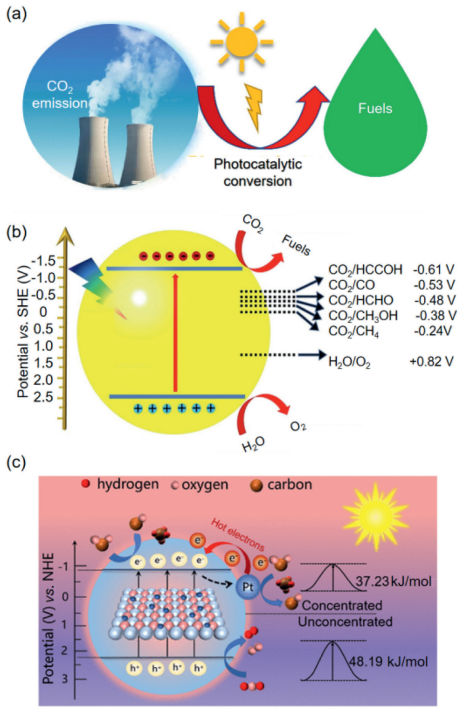


Fig. 4. (a) The schematic process of solar light driven photocatalytic CO_2 conversion and the advantages. (b) The scheme of photocatalytic CO_2 conversion into various products with different photoredox potentials. (c) The scheme of photothermal catalytic CO_2 conversion with lower activation energy.

processes, which together increase the rate of catalytic reactions and enable effective CO_2 conversion under relatively mild conditions (Fig. 4c) [71]. As a type of photothermal catalysis, introducing thermal energy into photocatalysis can improve the utilization efficiency of sunlight, promote the excitation and separation of photoinduced charge carriers, accelerate the diffusion of reaction molecules, and enhance the reaction performance [72,73].

3. Preparation of photonic crystals with slow photons effect

The preparation of uniform and high-quality photonic crystals is of great importance for the investigation of slow photons effect and application of photocatalytic fields. Specifically, creating an ordered three-dimensional macroporous structure is crucial as it approaches the complete photonic bandgap. This bandgap signifies that photonic crystals can reflect light in all directions of propagation within a specific frequency range. Up to now, there are two major approaches to fabricate photonic crystal materials: bottom-up method and top-down method.

3.1. Bottom-up method

The bottom-up method has been extensively adopted for synthesizing nanostructured materials with different morphology, which includes hydrothermal/solvothermal method, molecule self-assembly, co-precipitation method, sol gel method [74,75]. For the fabrication of photonic crystals, self-assembly and manual assembly techniques have been frequently reported. In general, self-assembly is simple and easy to be conducted, and is widely used for preparing nanomaterial with various structure and morphology. Although nanoparticle self-assembly can produce photonic crystals with an opal structure, the refractive index ratio of photonic crystals is generally much lower to achieve a full bandgap [76]. Therefore, photonic crystals with an opal structure only exhibit a pseudo photonic bandgap. Differently, inverse opal structured materials are expected to achieve a complete photonic bandgap. Researchers applied the photonic crystal template method to prepare the nearly complete photonic band gap inverse opal structure. As shown in Fig. 5a, colloidal nanoparticles initially create ordered photonic crystals with an opal structure *via* a self-assembly process. Subsequently, either the penetration method or the original sub-layer deposition method is employed to fill the gaps in the photonic crystal template with solid materials. Finally, the original photonic crystal template is removed by the chemical dissolution or high-temperature calcination to generate photonic crystals with inverse opal structure. For instance, *via* changing the size of colloidal nanoparticles, the inverse opal TiO_2 materials with different sizes can be obtained (Figs. 5b–j), which exhibit different colors under daylight due to the scattering of light with different wavelengths. So far, various semiconductor materials with inverse opal structures, such as metal sulfides, metal oxides, and carbon materials, have been used for efficient photocatalytic reactions due to their unique slow photon effect [38,40].

3.2. Top-down method

The top-down strategy adopt physical or mechanical methods to reduce the size of bulk materials to the nanometer or micrometer scale, which mainly including mechanical drilling and photolithography methods [77]. Typically, Yablonovich *et al.* for the first time prepared a uniform photonic crystals with unique slow photons effect *via* direct mechanical drilling method [78]. This drilling technique for creating photonic crystals by mechanically drilling periodic holes in the substrate material, primarily applicable to macroscopic periodic structures on the millimeter to micrometer scale. Photolithography strategy is based on photochemical reactions and etching techniques, which enables high-precision control of photonic crystal structures and is widely used in the preparation of complex periodic structures [79,80]. Specifically, the photoresist occurs chemical change (such as crosslinking or decomposition) under light illumination, a preset periodic pattern is

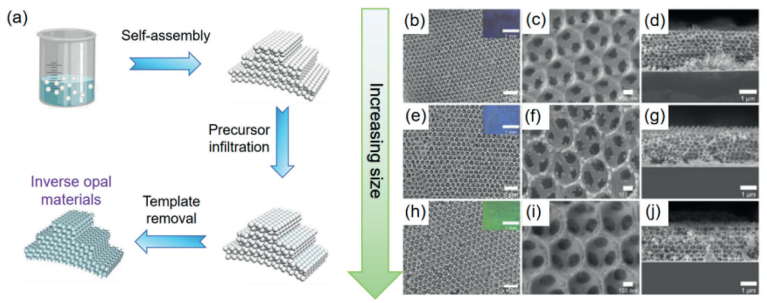


Fig. 5. The schematic process of colloidal template method for the preparation of inverse opal structures materials. The inverse opal TiO_2 materials with different sizes of (b-d) 370 nm, (e-g) 420 nm and (h-j) 460 nm obtained by template method. Reproduced with permission [11]. Copyright 2023, Elsevier.

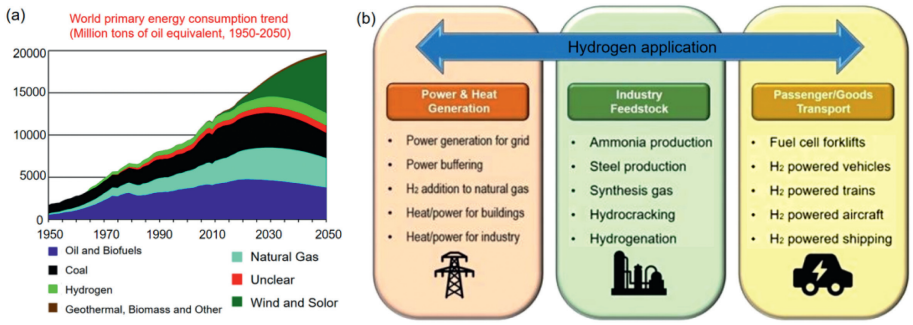


Fig. 6. (a) The different energy source consumption trends over the past few decades in the word. (b) The different application fields of the hydrogen energy.

transferred onto the photoresist through a mask plate, and then the pattern is loaded onto the substrate material through etching techniques, ultimately forming a photonic crystal with a periodic dielectric structure. In comparison to bottom-up method, the top-down strategy is relatively less reported for preparing photonic crystals for photocatalytic applications.

4. Slow photons for catalytic green energy conversion applications

Solar energy as the inexhaustible and renewable energy sources have aroused great interests in photocatalysis and photovoltaics fields [81]. However, the unsatisfactory solar energy conversion efficiency caused by the poor light absorption capability and inferior quantum conversion yield of materials restricted the advances of solar energy technology [82]. Although a variety of strategies have been developed to improve the utilization ability of sun light [83–85], the slow photons effect has been always ignored in material design. In this section, we systematically introduced the advanced progresses of designing photonic crystal structured materials with tunable slow photons effect and revealed the inherent mechanism of slow photons in accelerating photocatalytic green energy conversion.

4.1. Photocatalytic water splitting

The increasing fossil energy consumption and global energy shortage issue forces scientists to develop new carbon neutral energy sources (Fig. 6a) [86], especially of hydrogen energy, which is widely deemed as a green, sustainable and environmentally friendly energy feedstock, and applied in different fields in the word (Fig. 6b) [87]. Currently, there are various key methods for producing hydrogen, such as extracting hydrogen from fossil fuels, using electrolysis to split water, and innovative techniques like solar-driven water splitting, thermochemical water decomposition, and biomass hydrogen production [88]. Notably, solar-driven water splitting is particularly promising as it transforms light energy into chemical energy, allowing for storage and positioning it as a potential solution to the global energy crisis and environmental pollution issues.

At present, the most efficient solar powered water splitting for hydrogen generation is reached *via* coupling solar cells with water electrolysis devices (Fig. 7a) [89]. The solar to hydrogen (STH) energy conversion efficiency has been reported to be as high as 30 % (Fig. 7b). Differently, the energy conversion efficiency of photocatalytic water splitting for hydrogen production is much lower (only about 1 %). Nevertheless, the overall system design of photocatalytic hydrogen production is much simpler, the cost is lower, and it is easier to industrial scale, thus endowing promising commercial application prospects. As the core aspect of photocatalytic hydrogen production technology, photocatalyst materials directly decide the efficiency of the entire photocatalytic reactions. Therefore, the development, design, and modification of advanced photocatalysts have become a research hotspot in photocatalysis hydrogen evolution field.

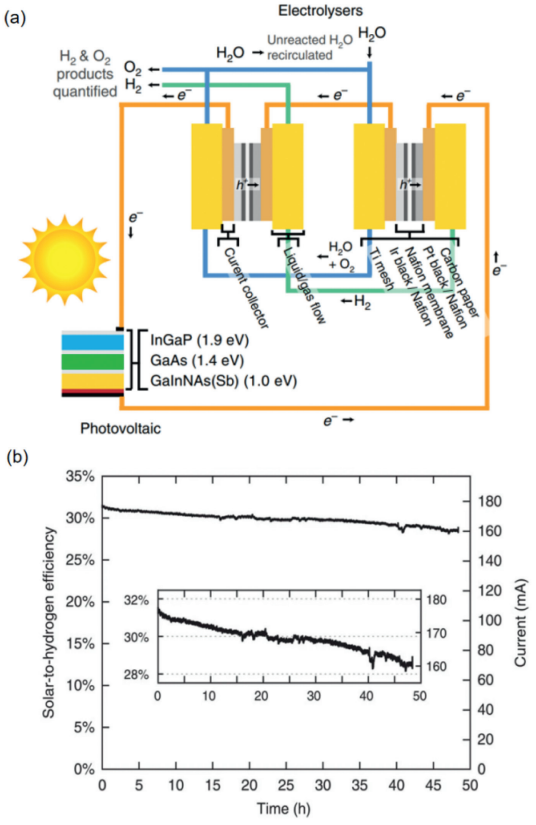


Fig. 7. (a) The scheme of sunlight driven water splitting *via* coupling solar cells with water electrolysis devices. (b) The solar to hydrogen energy conversion efficiency for long-term running. Reproduced with permission [89]. Copyright 2016, Springer Nature.

In past few years, Su's group has conducted a series of works to confirm the essential role of slow photons effect for boosting photocatalytic hydrogen production in aqueous solution by constructing various kinds of photonic crystal structured composites. In 2016, their group reported a ternary TiO_2-Au-CdS photocatalyst with uniform photonic crystal structure based on 3DOM TiO_2 for efficient photocatalytic water splitting to hydrogen generation [90]. The schematic process of the TiO_2-Au-CdS inverse opal synthesis is depicted in Fig. 8a. Firstly, the 3DOM TiO_2 was successively immersed into $HAuCl_4$ and citrate aqueous solution to uniformly decorate Au nanoparticles on the surface of 3DOM TiO_2.

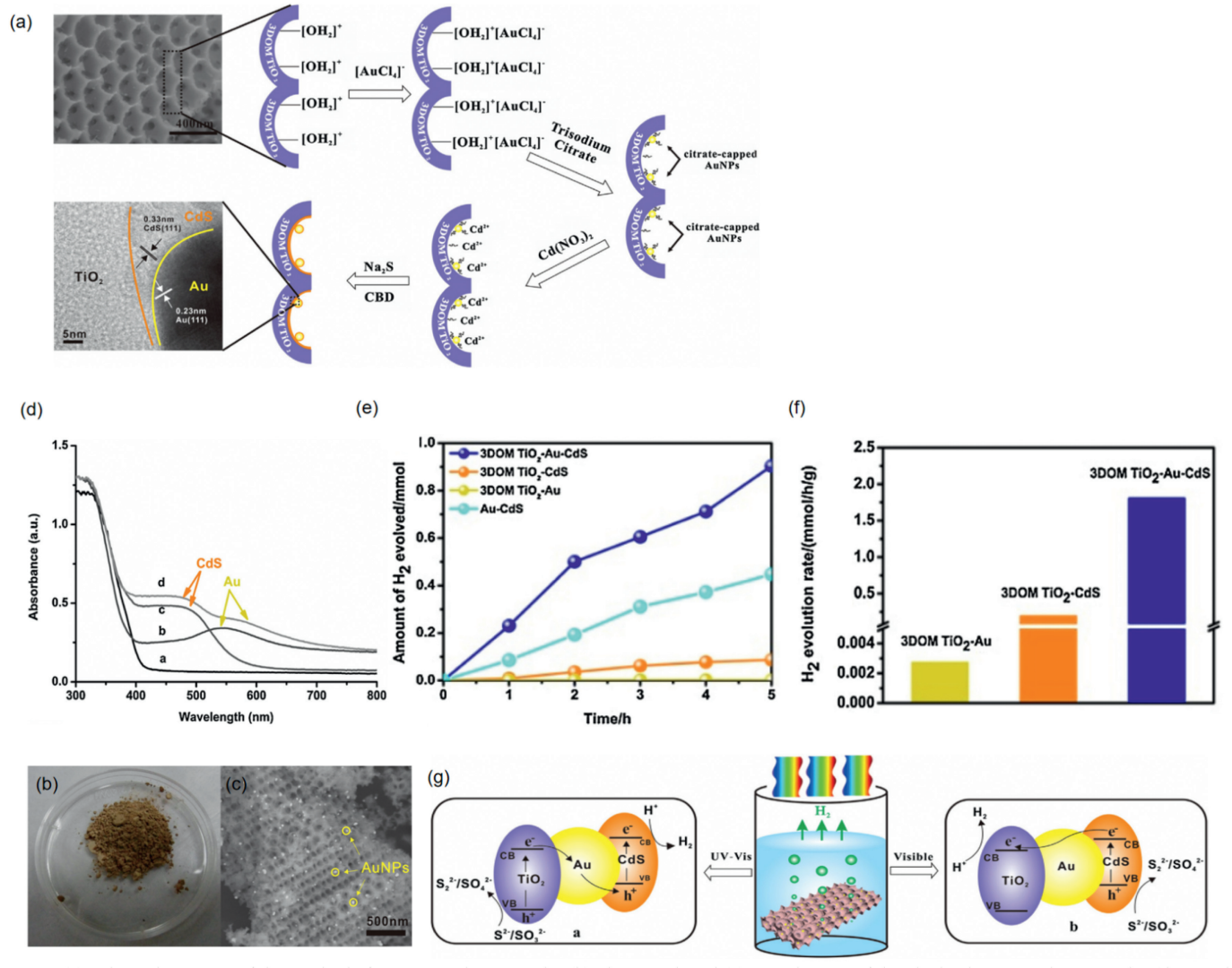


Fig. 8. (a) Schematic process of the synthesis for 3DOM TiO_2-Au-CdS. (b) Photograph and (c) SEM images of the obtained 3DOM TiO_2-Au-CdS. (d) UV–vis absorption spectra of the prepared photocatalysts. (e) Time-dependent photocatalytic hydrogen evolution and (f) hydrogen production rates of the obtained samples under visible light excitation. (g) The scheme of photocatalytic hydrogen evolution over inverse opal structured 3DOM TiO_2-Au-CdS upon UV-visible and visible light illumination. Reproduced with permission [90]. Copyright 2016, Elsevier.

Then the generated nanoparticles are encapsulated with citrate ions and would couple with Cd^{2+} ions because of the Coulomb force. Finally, S^{2-} ions replace citrate ions to generate CdS on the surface of Au nanoparticles and TiO_2. As shown in Fig. 8b, the prepared ternary 3DOM TiO_2-Au-CdS displays yellow color, indicating the considerable portion of visible-light harvesting. The SEM image indicates that the 3DOM TiO_2-Au-CdS exhibits a very uniform 3DOM structure, with gold nanoparticles approximately 30 nm in size distributed across the surface of the 3DOM TiO_2 (Fig. 8c). This arrangement can trigger a slow photo effect and surface plasmon resonance (SPR) phenomenon, enhancing the harvesting of visible light (Fig. 8d). As a result, the obtained 3DOM TiO_2-Au-CdS photocatalyst brings out efficient hydrogen generation rate of 1.81 mmol h^{-1} g^{-1} upon visible-light excitation, being 13 times greater than that of the binary TiO_2_CdS photocatalyst (Figs. 8e and f). The mechanism investigation illustrates that the photoinduced electrons on TiO_2 are transferred to recombine with the holes of CdS and under UV–visible light excitation, photoinduced electrons on CdS will couple with protons to generate hydrogen. Thus, the excellent hydrogen evolution over 3DOM TiO_2-Au-CdS sample can be ascribed to synergistic effect of the enhanced light harvesting by photonic crystal effect, the photosensitizing effect of Au and the prohibited rate of charge carriers recombination (Fig. 8g). Although the inverse opal photonic crystal structure can enhance light absorption through multiple scattering of incident light for efficient hydrogen evolution, the randomness of this scattering mode is difficult to quantitatively describe.

As discussed above, the slow photon effect is beneficial for enhancing the residence and absorption of light energy in materials, thereby enhancing photocatalytic hydrogen evolution performance. For a long time, the red edge slow photon effect has been considered to have a better photocatalytic enhancement effect than the blue edge slow photon effect. As a result, studies focused on improving photocatalytic performance through the slow photon effect primarily concentrate on the red edge slow photon effect, whereas investigations into the enhancement of photocatalytic performance *via* the blue edge slow photon effect are comparatively scarce. Therefore, further experiments are needed to demonstrate which of the red edge and blue edge slow photon effects is better in promoting photocatalytic performance. At present, researches on slow photon effects mainly focus on thin film samples with 3DOM structures. This is because thin film samples are easier to adjust

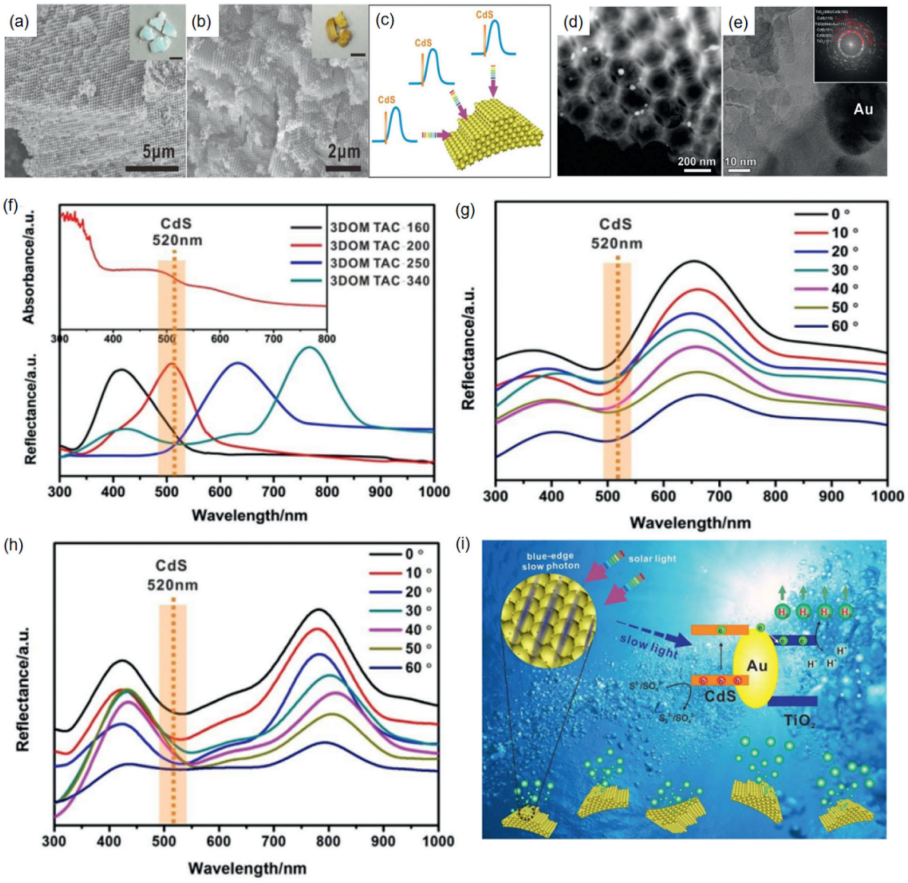


Fig. 9. SEM images of the prepared (a) TiO_2 inverse opal and (b) 3DOM TiO_2-Au-CdS samples (the insets show the photograph under day light). (c) The schematic diagram of irradiated light reflection simulation of 3DOM TiO_2-Au-CdS under various irradiation angles. (d) The HAADF-STEM and (e) HR-TEM images of the obtained 3DOM TiO_2-Au-CdS sample. (f) UV–vis reflectance spectra of 3DOM TiO_2-Au-CdS samples with different macropore sizes (the inset presents the absorption spectrum of CdS). UV–vis reflectance spectra of (g) 3DOM TAC-250 and (h) 3DOM TAC-160 samples at various incident light angles. (i) The scheme of the slow photon effect in 3DOM TiO_2-Au-CdS photocatalyst for hydrogen evolution upon visible-light irradiation. Reproduced with permission [94]. Copyright 2018, Elsevier.

the angle of incident light, thus can unveil the influence of incident light angle on slow photon effects [91,92]. Due to limitations in the preparation conditions of thin film samples, the effective mass of the samples is extremely low and difficult to control the film layer, resulting in generally poor photocatalytic performance [93]. How to achieve slow photon effects in 3DOM powder sample has become a long-standing challenge for researchers. The reason is that the orientation change of powder samples caused by continuous stirring during the photocatalytic liquid-phase reaction process can result in the slow photon effect not being able to continue to occur. Therefore, it is necessary to design 3DOM powder samples with specific framework and solve the problem of orientation change caused by stirring during liquid-phase reaction process, ensuring that the slow photon effect can continue to function.

In this context, their team developed a staircase-shaped 3DOM composite photocatalyst [94]. The self-assembly of PS nanospheres and template method are involved in this synthesis being similar to the aforementioned work, except that the obtained PS nanosphere template has a staircase-style configuration. From Fig. 9a, it can be seen that the synthesized TiO_2 inverse opal sample has a large area of intact 3DOM structure, and the staircase-style configuration is also clearly visible. The TiO_2 inverse opal with a size of 160 nm presents a blue color upon day light environment (inset of Fig. 9a), which is related to the periodic macroporous structure of the sample and the reflectance of blue light. The 3DOM structure and staircase-style configuration of the 3DOM TiO_2-Au-CdS sample remain intact after loading CdS and Au (Fig. 9b). The ternary 3DOM TiO_2-Au-CdS appears yellow color (inset of Fig. 9b) due to the yellow color of CdS itself covering the structural color of TiO_2 inverse opal. The staircase-shaped 3DOM composite helps minimize the impact of changes in the angle of incoming light on the reflection spectrum and preserves the slow photon effect during ongoing stirring (Fig. 9c). The HAADF-STEM (Fig. 9d) and HR-TEM (Fig. 9e) images demonstrate that the Au nanoparticles are well dispersed on the macropore of the obtained 3DOM photocatalyst. In order to illustrate the relationship between the structural color and pore size of the inverse opal structure, a series of 3DOM TiO_2 and 3DOM TiO_2-Au-CdS with different pore sizes were synthesized by changing the size of PS nanosphere template. At the boundary of the reflection spectrum, the propagation speed of the incident photons in the photonic crystal structure sharply decreases, and this part of the photons is called slow photons. When the energy of slow photons matches the energy corresponding to the bandgap width of the semiconductor materials, slow photons are absorbed by the semiconductor component. From the reflection spectra of 3DOM TiO_2-Au-CdS samples with different macropore sizes, it can be seen that the boundary positions of the reflection spectra are mostly in the visible light region (Fig. 9f). Therefore, when the energy of red edge slow photons or blue edge slow photons overlaps with the energy corresponding to the CdS bandgap width (about 2.4 eV), the slow photon effect will occur.

Due to the stirring during the photocatalytic hydrogen evolution process, the sample is in a randomly oriented state. To illustrate the relationship between the slow photon effect and the incident light angle of the synthesized powder sample, the reflection spectra of two different 3DOM TiO_2-Au-CdS samples were mea-

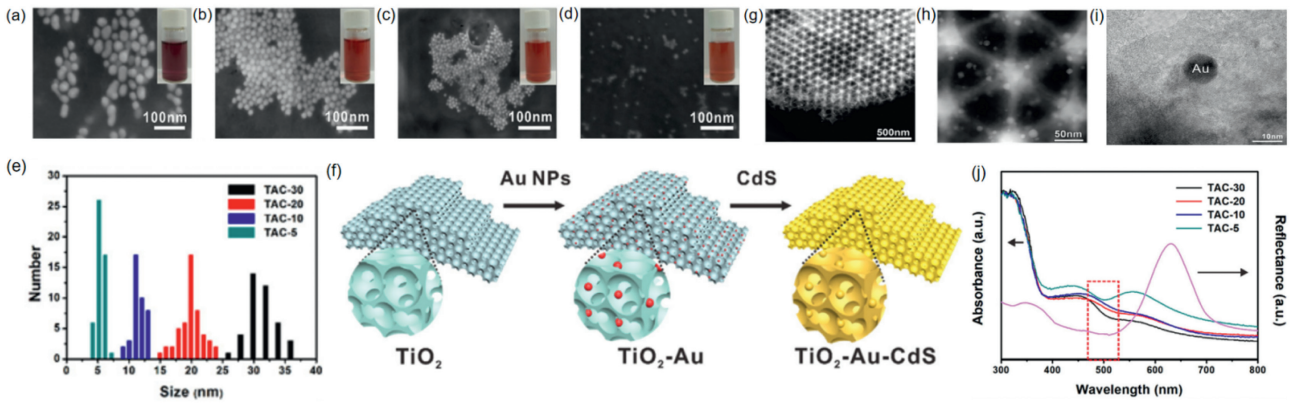


Fig. 10. SEM pictures of Au NPs with size of about (a) 30 nm, (b) 20 nm, (c) 11 nm, (d) 5 nm and the corresponding solution images. (e) Size distribution of the Au NPs. (f) The scheme of the synthesis of 3DOM TAC. (g, h) HAADF-STEM images and (i) HR-TEM pictures of 3DOM TAC-10 sample. (j) UV–vis absorption spectrum of 3DOM TAC with loading different sizes of Au and the reflectance spectra of TAC-30. Reproduced with permission [95]. Copyright 2021, Elsevier.

sured at different incident light angles (Figs. 9g and h). The findings show that the reflection spectrum of the solid 3DOM TiO_2-Au-CdS sample does not vary significantly with changes in the angle of incident light. This suggests that if a slow photon effect exists in the sample, it will continue to operate effectively throughout the photocatalytic hydrogen production process. The main reason is that the synthesized sample has a staircase-style structure, which avoids the orientation problem caused by the angle change of incident light, making the sample have the same structure in all directions. Differently, 3DOM TAC-250 has a blue-edge slow photon effect due to the overlap between the blue edge of reflection spectrum and absorption of CdS, whereas 3DOM TAC-160 presents a red edge slow photon effect, which could cause different photocatalytic activity.

To illustrate the effect of slow photon effect on the photocatalytic performance, visible-light photocatalytic hydrogen production was studied for the TiO_2-Au-CdS samples with different pore sizes. Due to the same specific surface area and mesoporous pore size distribution of the samples with different pore sizes, the factor causing differences in hydrogen production performance among different samples is the change in large pore size, which is the influence of slow photon effect. The reflection peak of sample 3DOM TAC-200 covers the intrinsic absorption region of CdS, indicating that the incident light that can be absorbed and utilized by CdS is majorly reflected by the inverse opal structure, resulting in poor hydrogen evolution performance (1.81 mmol h^{-1} g^{-1}). The hydrogen production rate over bulk TAC under visible light is 1.66 mmol h^{-1} g^{-1}, being inferior than that of 3DOM TAC-200. The findings indicate that although the 3DOM structure reflects a significant amount of the incident light that CdS can absorb, its ability to scatter light multiple times and facilitate rapid mass transfer enhances its photocatalytic performance compared to the TAC sample lacking the 3DOM structure. This highlights the importance of structural advantages in hydrogen production. The 3DOM TAC-160 sample exhibits a hydrogen production rate of 2.55 mmol h^{-1} g^{-1}, associated with the red-edge slow photon effect, while the 3DOM TAC-250 sample shows a hydrogen production rate of 3.50 mmol h^{-1} g^{-1}, linked to the blue edge slow photon effect. It can be deduced that the blue edge slow photon effect also has the capability to enhance photocatalytic performance, which is more obvious than the red edge slow photon effect. This discovery firstly confirmed that the blue-edge slow photon effect has a better photocatalytic performance enhancement effect than that of the red-edge slow photon effect. The primary reason is that during the occurrence of the red-edge slow photon effect, the light reflected by the structure consists of photons that have shorter wavelengths and higher energy. When the blue edge slow photon effect occurs, the incident light reflected by the structure is composed of photons with longer wavelengths or lower energy, which cannot be absorbed by the material. Therefore, from the perspective of the incident photon energy that can be effectively absorbed and utilized, the blue edge slow photon effect does have a better enhancement effect on photocatalytic performance (Fig. 9i).

Considering the special SPR effect and fantastic charge transfer performance of gold nanoparticles in the ternary TiO_2@Au@CdS system, this team conducted further work to study the effect of gold nanoparticles size on photocatalytic performance [95]. They precisely modulated the size of gold nanoparticles and systematically investigated the size effect of gold nanoparticles in the ternary 3DOM TiO_2@Au@CdS composites (Figs. 10a–i), achieving further improvement in the photocatalytic hydrogen generation. In their work, sodium citrate solution with different concentrations is used to reduce chloroauricacid to prepare Au nanoparticles of tunable particle sizes, and loaded them into a 3DOM TiO_2 framework. CdS was introduced in the ternary system as the photosensitive material through chemical bath deposition route. The prepared ternary materials with tunable Au nanoparticles size not only have the capability to absorb UV-visible light, but also effectively facilitate the photogenerated carriers dissociation *via* the constructed type II heterojunction. The UV–vis absorption and reflection spectra characterizations illustrated that TiO_2@Au@CdS composites with perfect photonic crystal structures also exhibit blue-edge slow photon effects (Fig. 10j), ensuring maximized utilization of incident photons by the photocatalyst. Photocatalytic tests demonstrated that there are significant differences in the photocatalytic H_2 evolution rate as changing the size of Au nanoparticles in the 3DOM TiO_2@Au@CdS system. The highest photocatalytic hydrogen production rate is achieved when the Au nanoparticles size is around 10 nm (Fig. 11a). A variety of photoelectrochemical characterizations were conducted to unveil the performance improvement mechanism. The photocurrent intensity gradually increases with decreasing the size of Au nanoparticles, indicating that the SPR effect of Au nanoparticles is gradually enhanced (Fig. 11b). The EIS tests also exhibit the same conclusion (Fig. 11c). However, electrochemical impedance spectroscopy (EIS) characterization gives rise to difference EIS results, and hydrogen production rate reveals a strong correlation between hydrogen production activity and charge transfer impedance. This suggests that altering the size of gold nanoparticles can influence hydrogen production efficiency by impacting both SPR and EIS characteristics, with EIS having a more significant effect. Additionally, the author utilized the finite time difference method to simulate the intensity and

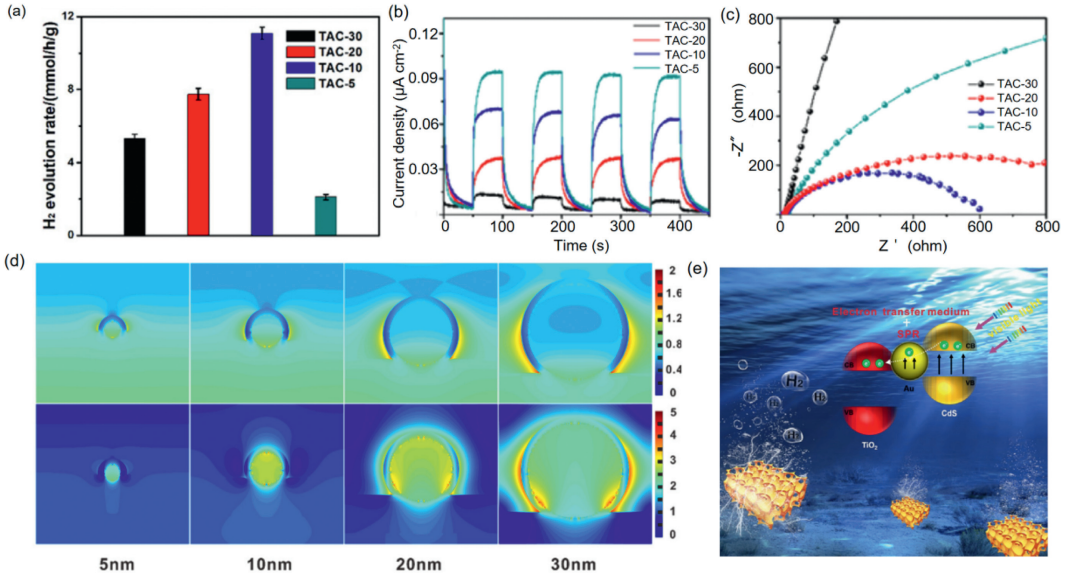


Fig. 11. (a) Photocatalytic hydrogen production rates over the 3DOM TAC with loading different sizes of Au. (b) photocurrent response and (c) EIS spectra of the obtained samples. (d) The simulated electromagnetic fields intensity distribution of the 3DOM TAC samples. (e) The schematic process of slow photons and SPR effects promoting photocatalytic hydrogen evolution. Reproduced with permission [95]. Copyright 2021, Elsevier.

distribution of the electromagnetic field within the ternary 3DOM TiO_2@Au@CdS system, based on structural analysis and electrochemical characterization findings (Fig. 11d). The electromagnetic field intensity was significantly enhanced at the interfaces between TiO_2-Au and Au-CdS, verifying that the charge transfer pathway follows the type II heterojunction mechanism under visible light conditions. It is important to note that when gold nanoparticles are very small (5 nm), the enhancement of electromagnetic field intensity at the interface is minimal, suggesting that charge transfer at the interface faces significant resistance in this scenario. Combined with the slow photon effect and optimized SPR effect of Au nanoparticles, a significant improvement in the photocatalytic hydrogen production performance of 3DOM TiO_2@Au@CdS catalyst system was achieved (Fig. 11e).

In a photocatalytic system, the heterojunction plays a crucial role in separating photoinduced electron-hole pairs. Therefore, it is important to thoroughly investigate the impact of the slow photon effect in three-dimensional ordered mesoporous (3DOM) heterostructure composites and to explore the advantages of combining slow photons with the heterojunction in photocatalytic hydrogen production systems [96–99]. Typically, Liu and co-workers prepared a series of CdS@ZnO core-shell inverse opal (CdS@ZnO-csIO) heterostructure photocatalyst for visible light driven hydrogen production [100]. In this composite photocatalyst, the utilization efficiency of photons is effectively enhanced and the separation of photogenerated charge carriers has been promoted, therefore improving the photocatalytic hydrogen evolution efficiency. As shown in Fig. 12a, they adopted the continuous ion layer adsorption reaction (SILAR) technique to uniformly decorate CdS nanoparticles onto the framework of ZnO inverse opal (ZnO-IO) and obtained CdS@ZnO-csIO composite photocatalyst. By adjusting the macropore size of ZnO-IO, the CdS@ZnO-csIO composites with different pore sizes were obtained (Figs. 12b–d), which can achieve the precise modulation of the photonic bandgap position in these inverse opal composites. Apparently, these CdS@ZnO-csIO inverse opal composites exhibit a uniform and stable inverse opal structure with macropore sizes and uniform pore walls. ZnO nanoparticles exhibit the same grain orientation at a certain scale, which facilitates the rapid migration of photogenerated electrons. Moreover, there is a tight contact interface between CdS and ZnO phases. The tight contact interface is also expected to result in efficient electron transfer and carrier separation efficiency. With increasing the size of the macropore, the reflection peaks shift towards longer wavelengths (Fig. 12e). The red-edge position of CdS@ZnO-csIO-230 and blue-edge position of CdS@ZnO-csIO-290 are located near the electronic band edge of CdS, providing great potential of slow-photon effect for promoting photocatalysis (Fig. 12f). The CdS@ZnO-csIO-290 photocatalyst displayed the enhanced hydrogen evolution rates of 48.7 mmol g^{-1} h^{-1} under simulated solar light irradiation (Fig. 12g). On account of VB-XPS and Mott Schottky characterization results, the CB and VB positions of ZnO and CdS components can be determined (Fig. 12h). And a type II heterojunction charge transfer pathway was existed in the CdS@ZnO-csIO composite photocatalyst for effect separation of photogenerated electrons and holes, endowing the reduction and oxidation reactions at two different reaction positions (Fig. 12i). This work further confirms the synergy of the slow photon effect and heterostructure in the photocatalysis system.

Overall, slow photon photocatalysis has shown many significant advantages in water splitting, including increasing light absorption, prolonging carrier lifetime, facilitating charge transfer, and expanding visible-light response range. It provides an effective way to improve the efficiency of photocatalytic water splitting and achieve efficient utilization of solar energy. However, slow photon photocatalytic water splitting still faces many challenges in practical applications, including the complexity of inverse opal structure design and preparation, the stability issues of macropore, and limitations in cost and scale production.

4.2. Photocatalytic CO_2 conversion

The rapid consumption of fossil fuels has caused a significant rise in CO_2 levels in the atmosphere, resulting in severe environmental issues like an intensified greenhouse effect and rising sea levels, which pose a major threat to human life and industry [101,102]. Converting CO_2 into sustainable energy and clean fuel *via* photocatalysis technique can not only reduce the amount of CO_2 in the atmosphere, but also alleviate the global energy shortage [103]. Enhancing the adsorption and activation of CO_2 and H_2O molecules, increasing the efficiency of capturing and utilizing in-

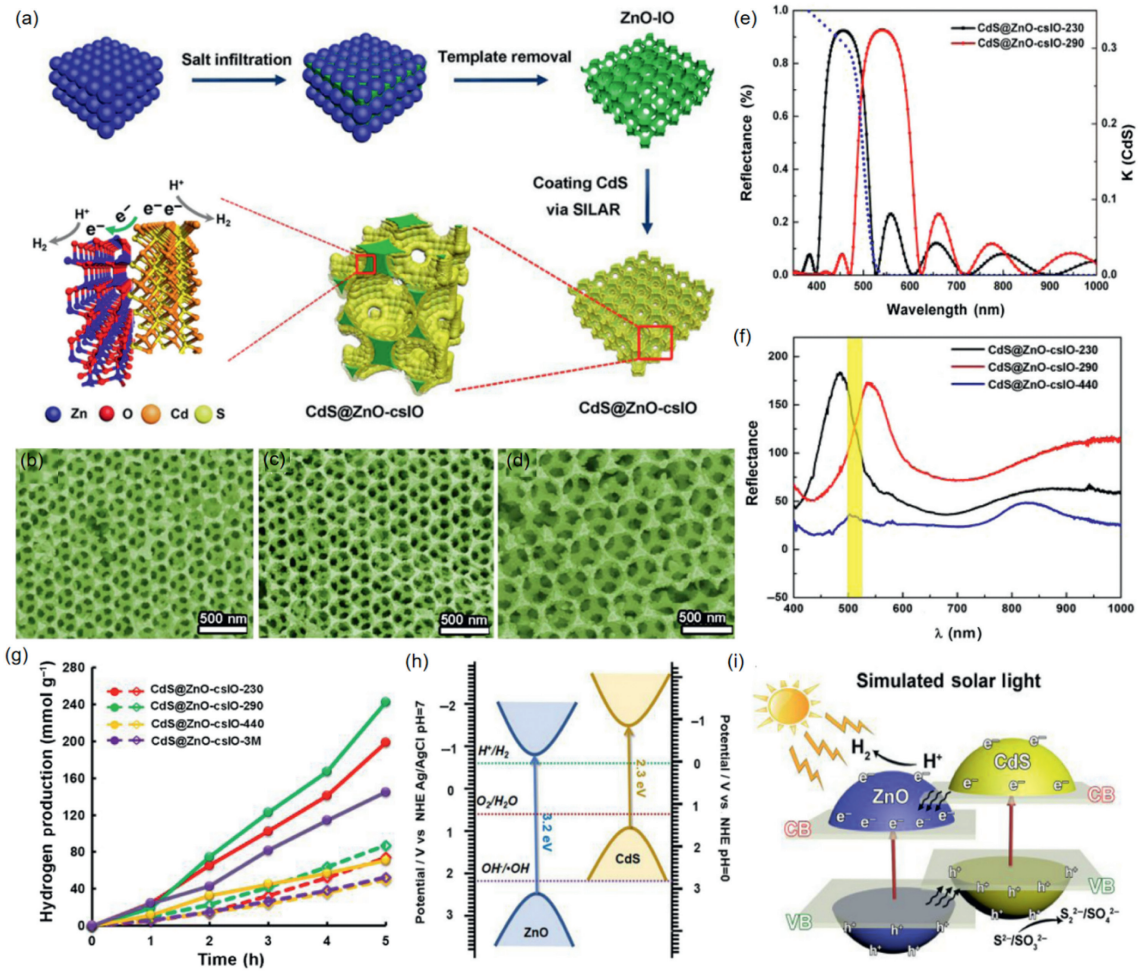


Fig. 12. (a) Schematic process of the synthesis of CdS@ZnO-csIO heterostructure. (b-d) The SEM pictures of the obtained CdS@ZnO-csIO heterostructures with different macropore sizes. The UV–vis reflectance spectra of (e) CdS@ZnO-csIO230 and (f) CdS@ZnO-csIO-290 inverse opal samples obtained *via* theoretical simulation. (g) Time-dependent photocatalytic hydrogen evolution over the prepared samples. (h) The specific energy level position of ZnO inverse opal and CdS component. (i) The schematic process of heterostructure for promoting charge shift in photocatalysis reaction. Reproduced with permission [100]. Copyright 2021, Chinese Chemical Society.

coming photons, and encouraging the dissociation of photogenerated carriers are crucial factors in advancing photocatalytic CO_2 conversion [104,105].

In this context, Zhao's team introduced a photonic crystal composite photocatalyst (PC GDY-Cu/ZnO) that features a graphdiyne (DGY) loaded with a Z-type heterojunction. This catalyst demonstrates highly effective photocatalytic conversion of CO_2 into CH_4, thanks to its distinctive slow photon effect, pore properties, and structural advantages [106].

As shown in Fig. 13a, the PC GDY-Cu/ZnO composite photocatalyst can be prepared by inducing *in-situ* growth of GDY on the surface of PC Cu/ZnO. The introduction of GDY component and oxygen vacancies in ZnO can enhance the adsorption and activation capability of CO_2 molecules, thereby promoting the entire photoreduction of CO_2. By modifying the dimensions of the large pores in the photonic crystal composite (Figs. 13b and c), the increased absorption of visible light following the addition of GDY aligns closely with the slow photon region at the red edge (Fig. 13d). This alignment enhances the capture and use of visible light, thereby boosting photocatalytic activity. The schematic slow photons effect and electron transfer pathway of PC GDY-Cu/ZnO photocatalyst are depicted in Figs. 13e and f. The GDY component is uniformly dispersed on the PC GDY-Cu/ZnO framework, significantly enhancing the visible-light absorption in the range of 400–550 nm. By adjusting the position of the photonic bandgap, the red edge slow photons region of PC GDY-Cu/ZnO overlaps with the visible-light response range of GDY, greatly improving the refraction of photons on the cavity surface and thus enhancing the absorption and utilization of visible-light. Under the enhanced light harvesting of slow photons effect, the photoinduced electrons on ZnO and GDY are rapidly excited, and the electrons on ZnO are quickly transferred to GDY through the Z-type heterojunction, thus improving the separation efficiency of photoinduced electrons and holes. Moreover, the oxygen vacancies generated by hydrogen reduction on the surface of PC GDY-Cu/ZnO enhance the adsorption and activation ability of H_2O and CO_2 molecules. In summary, the photogenerated carrier separation efficiency of PC GDY-Cu/ZnO composite has been improved by 10.3 times, and the adsorption ability for CO_2 and H_2O molecules has been increased by 32.5 and 2.2 times in comparison to pure ZnO, respectively. Driven by slow photons effect, the increased CH_4 yield of PC GDY-Cu/ZnO photocatalyst is 33.67 μmol g^{-1} h^{-1}, with a desirable product selectivity of 93.3 %.

In addition, their group also reported a Ti-F bond bridged IL-CuCQDs-F/TiO_2 inverse opal composite photocatalyst (IO–CFTi) (Fig. 13g) [107], which can promote photoreduction of CO_2 by the synergy of slow photons effect and Ti-F bond. Firstly, EDTA (Cu) and ionic liquid [HOEtMIM] [BF_4] are used to prepare modified carbon quantum dots (IL-CuCQDs-F), which can grow on the surface of TiO_2 photonic crystal substance by virtue of the intense Ti-F bonds. The IL-CuCQDs-F can effectively extend light absorption from UV to the visible light region. Meanwhile, the Ti-F bond between the interface of IL-CuCQDs-F and TiO_2 photonic crystal facilitates

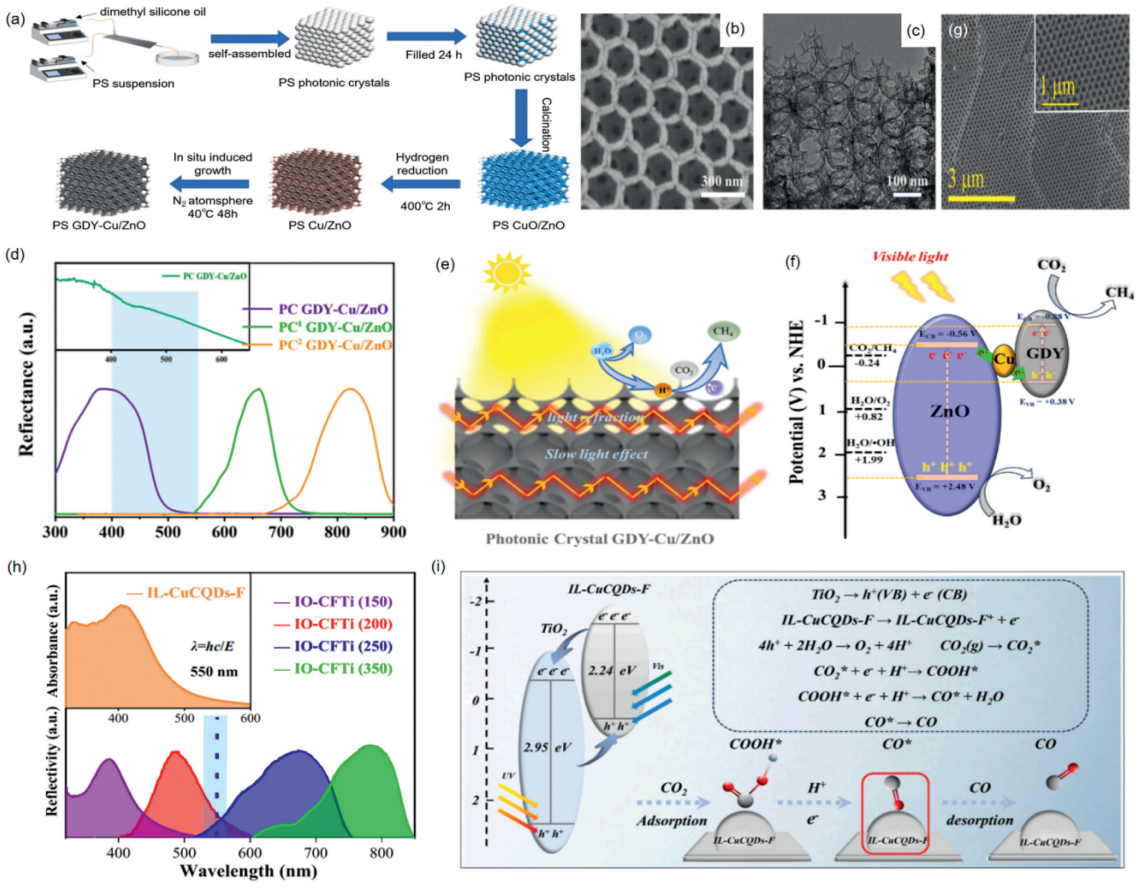


Fig. 13. (a) Schematic process of the synthesis of PC GDY-Cu/ZnO composite photocatalyst. (b) SEM and (c) TEM images of the prepared PC GDY-Cu/ZnO sample. (d) The reflectance spectra of PC GDY-Cu/ZnO with different macropore sizes and the absorption spectra of PC GDY-Cu/ZnO (inset). (e) Schematic process of slow photons effect in efficient photocatalytic CO_2 reduction over PC GDY-Cu/ZnO photocatalyst and (f) the corresponding electron energy level with charge shift route. Reproduced with permission [106]. Copyright 2024, Elsevier. (g) SEM image of IO–CTi sample. (h) The reflectance spectra of O–CTi with different macropore sizes. (i) The scheme of the dissociation and migration of photoinduced charge and CO_2 molecule activation process over the IO–CFTi photocatalyst. Reproduced with permission [107]. Copyright 2025, Elsevier.

the photogenerated electron transfer from TiO_2 to CO_2 molecules, thereby providing enough reducing potential in this composite system. More importantly, the electronic excitation wavelength region of IL-CuCQDs-F is overlapped with the blue-edge of TiO_2 photonic crystal (Fig. 13h), leading to an improved slow photon effect. Thus, the light harvesting is drastically elevated *via* increasing the effective optical path length for efficient photocatalytic activity.

The photocatalytic CO_2 reduction mechanism of the obtained IO–CFTi composite photocatalyst is depicted in Fig. 13i. Under UV light irradiation, IO CFTi can form photogenerated electron-hole pairs. The CB position of IL-CuCQDs-F (−1.6 eV) is more negative than that of TiO_2 (−0.6 eV), indicating that the photoinduced electrons of IL-CuCQDs-F can be transferred to the CB of TiO_2, thereby achieving effective separation of photogenerated electrons. Firstly, CO_2 molecules are adsorbed by IL-CuCQDs-F and activated into CO_2^* intermediates. Then the adsorbed CO_2^* is reduced by coupling photogenerated electrons and protons, generating the COOH* intermediates, which undergo further reduction by accepting electrons and protons, releasing CO* and H_2O. Finally, CO* is desorbed from the surface of photocatalyst and converted into CO product. A robust Ti-F bond was established between the interface of IL-CuCQDs-F and TiO_2 inverse opal, accelerating the separation and rapid migration of photogenerated electron-hole pairs. As a result, the synthesized IO CFTi presents an increased CO generation rate of 78.1 μmol g^{-1} h^{-1} *via* photoreduction of CO_2, being about 50 times higher than that of the pristine TiO_2 photocatalyst.

In a whole, efficient photocatalytic CO_2 reduction can be achieved by slow photon effect due to its obvious merits in increasing light absorption, prolonging carrier lifetime, facilitating interface charge transfer, and enhancing product selectivity. Nevertheless, some challenges should be considered and addressed before the practical applications of this technique, including the separation of reduced products, stability issues in photocatalysts and limitations in cost and scale production.

4.3. Photothermal catalytic CO_2 conversion

In comparison to single photocatalysis, thermal-assisted photocatalytic reactions (photothermal catalysis) present much higher CO_2 conversion performance. In particular, thermal energy plays a significant role in reducing the activation energy of CO_2 molecule in catalytic reactions [108]. Moreover, the fast separation and transport of photogenerated charges can be achieved with the existence of thermal energy. Photothermal catalysis can combine the advantages of thermochemistry and photochemistry, where the synergistic effect of light energy and heat energy promotes the total reaction progress [109]. In photothermal reactions, heat can be generated by photothermal materials (self-heating) and external auxiliary heating [110]. Recently, photocatalysts with full spectrum absorption to harvest solar energy and achieve photothermal effects under sunlight irradiation has received more and more attention.

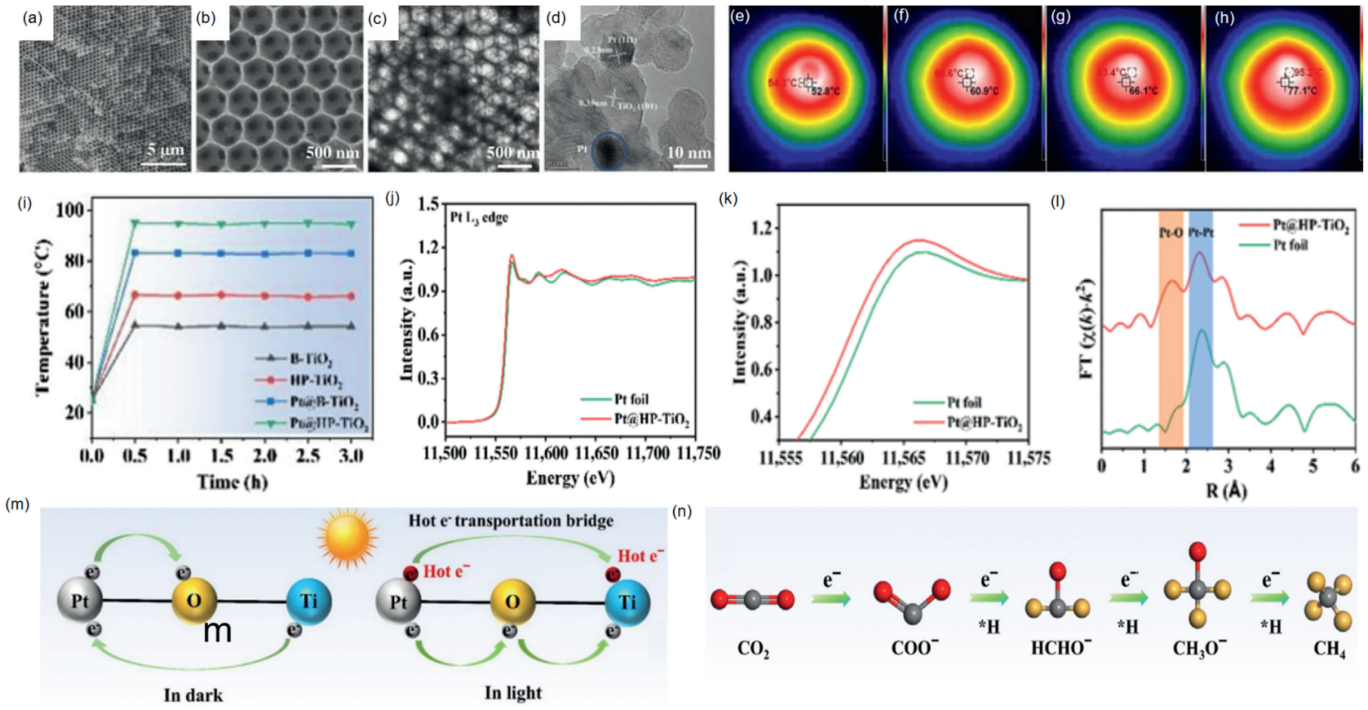


Fig. 14. (a, b) SEM images of the prepared Pt@HP-TiO_2. (c) TEM and the corresponding (d) HR-TEM images of Pt@HP-TiO_2. The infrared thermographies of (e) B-TiO_2, (f) HP-TiO_2, (g) Pt@B-TiO_2 and (h) Pt@HP-TiO_2 under Xe lamp illumination. (i) Time-dependent reaction temperatures of the prepared samples. (j, k) Pt L_3-edge XANES spectra and (l) Pt L_3-edge FT EXAFS spectra of the obtained Pt@HP-TiO_2 photocatalyst. (m) The charge and hot electron transfer route under different conditions. (n) The proposed photoreduction of CO_2 pathways on the Pt@HP-TiO_2 photothermal catalyst. Reproduced with permission [111]. Copyright 2025, Chinese Chemical Society.

Typically, Jiang and co-workers fabricated Pt nanoparticles loaded TiO_2 photonic crystal (Pt@HP-TiO_2) composite photothermal catalyst for efficient CO_2 conversion [111]. This composite catalyst couples the merits of slow photon effect, Pt-Ti hot electron transportation bridge, Pt nanoparticles induced SPR effect, and fast mass diffusion by rich pore structure. As depicted in Figs. 14a–d, the fabricated Pt@HP-TiO_2 composite possesses periodic macropores and interconnected pores in inner space, which can enhance irradiated light utilization due to the slow photon effect and present fast mass diffusion. The higher reaction temperatures of Pt-loaded TiO_2 compared with those of bare TiO_2 sample implied that the Pt nanoparticles triggered improved visible light absorption and elevated the reaction temperature. In comparison to B-TiO_2 and Pt@B-TiO_2 samples, Pt@HP-TiO_2 and HP-TiO_2 presented higher reaction temperatures (Figs. 14e–i), indicating that the 3DOM structured TiO_2 can harvest more UV light. The local heating induced by slow photons and SPR effects can accelerate the conversion of CO_2 molecules.

The X-ray absorption near-edge spectroscopy (XANES) spectra indicated that the intense electronic Pt-TiO_2 interaction existed in Pt@HP-TiO_2 due to electron transport between Pt particles and O atoms (Figs. 14j and k). The Fourier-transformed extended X-ray absorption fine structure (FT EXAFS) characterization (Fig. 14l) illustrated that the Pt-O bonds in Pt@HP-TiO_2 photothermal catalyst could promote charge shift between Pt nanoparticles and TiO_2 through the "Pt-Ti" interaction. Based on the aforementioned analysis, the authors put forth a proposed electron transfer pathway for Pt@HP-TiO_2 in both dark and light conditions (Fig. 14m). In the absence of light, the electrons are transferred from Pt to O *via* the "Pt-O" bond driven by the robust metal-support interaction between Pt and TiO_2. Meanwhile, the electrons in Ti migrate to Pt due to the difference in work function and Fermi level. Under visible light irradiation, the hot electrons overstep the Schottky barrier and are transferred from Pt to Ti *via* the efficient "Pt-Ti" hot electron transportation bridge. Additionally, the photogenerated electrons are excited from O to Ti. The efficient "Pt-Ti" hot electron transportation bridge is responsible for the remarkable photothermal catalytic reduction of CO_2 observed in this system. Finally, *in-situ* diffuse reflectance infrared Fourier transform spectra were performed to elucidate the reaction intermediates involved in the photothermocatalytic CO_2 reduction. The authors provided a comprehensive account of the CO_2 conversion pathway over Pt@HP-TiO_2 driven by the photothermal effect. The conversion of CO_2 follows a pathway: $CO_2 \rightarrow COO^- \rightarrow HCHO^- \rightarrow CH_3O^- \rightarrow CH_4$ (Fig. 14n). The high selectivity of CO_2 conversion into CH_4 on Pt@HP-TiO_2 induced by the hot electron transportation bridge and photothermal effect (Fig. 1l), as demonstrated in their work is a reliable and excellent result. The combination of the "Pt-Ti" hot electron transportation bridge, structure advantages, and photothermal effect, resulted in a CH_4 evolution rate of 29.68 μmol h^{-1} g^{-1} for Pt@HP-TiO_2 (Fig. 1h), which was significantly higher than that of bulk TiO_2 sample.

In summary, slow photons induced photothermal catalytic CO_2 conversion has significant advantages, which is considered as a highly promising approach for the resource utilization of CO_2. However, this technology also has problems such as complex thermal management, poor catalyst stability, unclear reaction mechanism, and high cost of noble metal utilization. Thus, the in-depth research on the design and preparation of photothermal catalysts with high stability and low cost should be conducted. Meanwhile, the advanced characterizations and theoretical calculation methods to explore the mechanism of the synergistic effect of light and heat is necessary to provide theoretical guidance for the optimization of catalysts and reaction systems.

5. Outlooks and challenges

In this review, the basic principles of the slow photon effect in inverse opal structured materials for photocatalysis and photothermal catalysis are comprehensively summarized. Meanwhile, the

preparation methods, structure properties of inverse opal structured materials, as well as their advantages on photocatalytic and photothermal catalytic reactions are discussed. When compared to other types of porous structures, the inverse opal structure offers a greater specific surface area, numerous active surface sites, and superior performance in photoinduced charge migration. Additionally, it provides a distinctive slow photon effect, which is essential for boosting light absorption and enhancing photocatalytic activity. In addition, photocatalytic water splitting and CO_2 reduction under the effective slow photons effect were thoroughly summarized. In recent years, although significant research progress has been achieved in the field of photocatalysis using inverse opal structured materials, there is still a long way to go before commercial applications, and further research is still needed in many aspects.

(1) Photonic crystals with unique periodic structures can promote photon capture and control the interaction between light and materials, thereby improving the light utilization efficiency of semiconductor photocatalyst materials. However, their light response is mainly located at UV and visible-light regions and limits the solar full spectrum photocatalysis. It is meaningful to extend the light-harvesting range of photonic crystal catalysts to the infrared region. The fabrication of a donor-acceptor system to broaden the light absorption of materials should be a good solution to improve the quantum efficiency of solar energy conversion.
(2) As to the fabrication process, although the high activity of inverse opal materials has been prepared in the laboratory, their catalytic performance is still far from meeting industrial standards, and it is indeed very difficult to produce uniform inverse opal structures on an industrial scale. Meanwhile, a series of routes have been reported for the preparation of inverse opal structure, but the template method remains the main approach, thus the operation is cumbersome and the procedure is complex. In this regard, further research should be conducted on manufacturing large-scale and uniform inverse opal structures through facile template-free routes.
(3) Improving the stability of these pore structure for long-term photocatalytic reaction is one of the key challenges in the field of photocatalysis. By introducing stable coatings or functional groups on the surface of porous materials, the active components can be isolated from direct contact with corrosive substances, which is favorable for improving the stability of these pore structure.
(4) Finally, the *in-situ* spectroscopy techniques are suggested to track the dissociation and shift of photogenerated charges, to better understand the charge migration pathway and reaction mechanism. Meantime, it is suggested that machine learning could be employed to further investigate the relationship among slow photon effect, electronic structure, and charge shift, thereby offering theoretical views for photocatalytic sustainable energy evolution.

In the long run, slow photos induced efficient photocatalytic technology has undeniable potential under the "dual carbon" goal. With the continuous breakthrough and improvement of technology, it is expected to achieve large-scale application in the fields of energy production and environmental remediation, contributing an important force to global sustainable development. We sincerely hope that this critical review can provide researchers with fundamental knowledge and inspire innovative concepts in the synthesis of inverse opal materials for solar energy conversion.

This review presented the recent progress of for slow photons effect in photocatalysts for efficient photo/photothermocatalytic solar fuel production including water splitting and CO_2 conversion.

Declaration of competing interest

The authors declare that they have no known competing financial interests or personal relationships that could have appeared to influence the work reported in this paper.

Acknowledgments

This work was financially supported by the National Natural Science Foundation of China (Nos. 22402044 and 22406169), Zhejiang Provincial Natural Science Foundation of China (Nos. LQ24E020011 and LQ24B070001). Zhejiang Education Department of China (No. Y202352478) and Basic Research Expenses of Zhejiang Gongshang University (No. QRK23025) were also thanked.

References

[1] X. Li, S. Wang, L. Li, Y. Sun, Y. Xie, J. Am. Chem. Soc. 142 (2020) 9567–9581.
[2] J. Liu, H. Shi, K. Yu, et al., Chin. Chem. Lett. 34 (2023) 108274.
[3] H. Li, R. Li, G. Liu, et al., Adv. Mater. 36 (2024) 2301307.
[4] Y. Ding, S. Maitra, C. Wang, et al., Interdiscip. Mater. 1 (2022) 213–255.
[5] X. Shi, L.N. Cao, M. Chen, Y. Huang, Chin. Chem. Lett. 33 (2022) 5023–5029.
[6] A. Fujishima, K. Honda, Nature 238 (1972) 37–38.
[7] Y. Ding, S. Maitra, S. Halder, et al., Matter. 5 (2022) 2119–2167.
[8] H. Li, R. Li, Y. Jing, et al., ACS. Catal. 14 (2024) 7308–7320.
[9] T.R. Mogan, J. Zhang, L.S. Ng, et al., Angew. Chem. Int. Ed. 63 (2024) e202401277.
[10] Y. Ding, C. Wang, S. Bandaru, et al., J. Colloid. Interface Sci. 672 (2024) 600–609.
[11] T. L.Madanu, S.R. Mouchet, O. Deparis, et al., J. Colloid. Interface Sci. 634 (2023) 290–299.
[12] X. Yu, Z. Yu, H. Zhao, I.D. Gates, J. Hu, Chem. Synth. 3 (2023) 3.
[13] Y. Ding, C. Wang, L. Pei, et al., Inorg. Chem. Front. 10 (2023) 3756–3780.
[14] C. Wang, Z. Xie, Y. Wang, et al., Adv. Sci. 11 (2024) 2402471.
[15] R. Li, H. Li, X. Zhang, et al., Adv. Funct. Mater. 34 (2024) 2402797.
[16] C. Wang, H. Huang, B. Weng, et al., Appl. Catal. B: Environ. 301 (2022) 120760.
[17] Y. Ding, G. Yang, Z. Xiang, et al., J. Environ. Chem. Eng. 12 (2024) 113483.
[18] C. Wang, Y. Ding, Y. Wang, et al., Carbon Energy 6 (2024) e500.
[19] Y. Ding, Y. Ye, C. Wang, et al., J. Clean. Prod. 450 (2024) 142041.
[20] Y. Ding, G. Yang, S. Zheng, et al., J. Environ. Manage 366 (2024) 121875.
[21] C. Wang, Y. Ding, Z. Xie, et al., ACS. Mater. Lett. 7 (2025) 610–619.
[22] X. Jiang, R. Chen, Y.X. Chen, et al., Chem. Synth. 4 (2024) 46.
[23] L. Pei, Z. Luo, X. Wang, et al., J. Colloid. Interface Sci. 652 (2023) 636–645.
[24] J. Liu, H. Zhao, M. Wu, et al., Adv. Mater. 29 (2017) 1605349.
[25] Y. Ding, C. Wang, N. Han, et al., Chem. Synth. 4 (2024) 59.
[26] T. Baba, Nat. Photo 2 (2008) 465–473.
[27] J.I. Chen, G. Freymann, S.Y. Choi, et al., J. Mater. Chem. 18 (2008) 369–373.
[28] X. Zhang, Y. Liu, S.T. Lee, et al., Energy Environ. Sci. 7 (2014) 1409–1419.
[29] S. Zhou, R. Tang, L. Yin, Adv. Mater. 29 (2017) 1703682.
[30] J.I. Chen, G. Freymann, S.Y. Choi, et al., Adv. Mater. 18 (2006) 1915–1919.
[31] Y. Ding, C. Wang, R. Zheng, et al., EnergyChem 4 (2022) 100081.
[32] Y. Ding, L. Huang, T. Barakat, B.L. Su, Adv. Mater. Interfaces 8 (2021) 2001879.
[33] C. Zhang, K. Yu, Y. Feng, et al., Appl. Catal. B: Environ. 210 (2017) 77–87.
[34] Y. Ding, C.H. Wang, J.S. Zhong, et al., Sci. China Chem. 66 (2023) 1886–1904.
[35] M. Zalfani, B. van der Schueren, Z.Y. Hu, et al., J. Mater. Chem. A 3 (2015) 21244–21256.
[36] Y. Du, L. Zhou, Z. Liu, L. Yang, J. Porous Mater. 28 (2021) 109–116.
[37] H. Zhao, J. Liu, C.F. Li, et al., Adv. Funct. Mater. 32 (2022) 2112831.
[38] R.T. Guo, X. Hu, X. Chen, et al., Small 19 (2023) 2207767.
[39] C. Zhang, D. Yu, C. Peng, et al., Appl. Catal. B: Environ. 319 (2022) 121946.
[40] F. Wen, W. Liu, J. Mater. Chem. A 9 (2021) 18129–18147.
[41] M. Fan, J. Guo, G. Fang, et al., Chem. Synth. 4 (2024) 36.
[42] Z. Ma, X. Liu, X. Wang, et al., Chem. Eng. J. 468 (2023) 143569.
[43] Y. Lin, L. Gan, X. Zhao, et al., Chem. Synth. 5 (2025) 4.
[44] C. Wang, Y. Ding, B. Liu, et al., Chem. Commun. 59 (2023) 3122–3125.
[45] Y. Ding, S. Maitra, C. Wang, et al., Sci. China Mater. 66 (2023) 179–192.
[46] C. Wang, B. Weng, Y. Liao, et al., Chem. Commun. 58 (2022) 10691–10694.
[47] W.B. Yu, H.R. Zhang, H.W. Zhang, et al., Adv. Funct. Mater. 34 (2024) 2410816.
[48] Y. Ding, S. Maitra, D.A. Esteban, et al., Cell Rep. Phys. Sci. 3 (2022) 100874.
[49] C. Wang, B. Weng, M. Keshavarz, et al., ACS Appl. Mater. Interfaces. 14 (2022) 17185–17194.
[50] Y. Ding, L. Liang, N. Han, et al., J. Environ. Chem. Eng. 12 (2024) 113111.
[51] Y.F. Huang, M.J. Ran, Z.R. Li, et al., ACS Appl. Energy Mater. 7 (2024) 7818–7828.
[52] M.J. Ran, M. Wang, Z.Y. Hu, et al., J. Mater. Sci. Technol. 212 (2025) 182–191.
[53] Z.Y. Jiang, M.J. Ran, K. Liu, et al., Mater. Today Chem. 39 (2024) 102135.
[54] Y. Quan, R. Li, X. Li, et al., Small 20 (2024) 2406576.
[55] S. Qu, H. Wu, Y.H. Ng, ACS Catal. 14 (2024) 5297–5304.
[56] S. Cao, C. Wang, J. Fu, et al., ChemSusChem 10 (2017) 4306–4323.
[57] Y. Lee, J. Suntivich, K.J. May, et al., J. Phys. Chem. Lett. 3 (2012) 399–404.
[58] L. Lin, V. Polliotto, J. Vequizo, et al., ChemPhotoChem 6 (2022) e202200209.
[59] J. Ma, N. Sun, X. Zhang, et al., Catal. Today 148 (2009) 221–231.

[60] Z. Gao, J. Li, Z. Zhang, W. Hu, Chin. Chem. Lett. 33 (2022) 2270–2280.
[61] S. Jia, M. Dong, Q. Zhu, et al., Chem. Synth. 4 (2024) 60.
[62] J. Gao, S. Shiong, Y. Liu, Chem. Eng. J. 472 (2023) 145033.
[63] S. Mehla, A.E. Kandjani, R. Babarao, et al., Energy Environ. Sci. 14 (2021) 320–352.
[64] L. Pei, X. Wang, H. Zhu, et al., ACS Appl. Mater. Interfaces 15 (2023) 51300–51308.
[65] J. Ran, M. Jaroniec, S.Z. Qiao, Adv. Mater. 30 (2018) 1704649.
[66] J. Yang, C. Bie, Chem. Synth. 4 (2024) 2–7.
[67] Y. Ding, S. Maitra, C. Wang, et al., J. Energy Chem. 70 (2022) 236–247.
[68] Y. Yin, X. Kang, B. Han, Chem. Synth. 2 (2022) 12–20.
[69] L. Pei, Y. Yuan, W. Bai, et al., ACS Catal. 10 (2020) 15083–15091.
[70] W.A. Thompson, E. Sanchez Fernandez, M.M. Maroto-Valer, ACS Sustain. Chem. Eng. 8 (2020) 4677–4692.
[71] M. Wu, Y. Ren, F. Zhu, et al., Ind. Eng. Chem. Res. 62 (2023) 9463–9473.
[72] J. Zhang, H. Chen, X. Duan, et al., Mater. Today 68 (2023) 234–253.
[73] D. Mateo, J.L. Cerrillo, S. Durini, J. Gascon, Chem. Soc. Rev. 50 (2021) 2173–2210.
[74] D. Mijatovic, J.C. Eijkel, A. van den Berg, Lab. Chip. 5 (2005) 492–500.
[75] N. Abid, A.M. Khan, S. Shujait, et al., Adv. Colloid. Interface Sci. 300 (2022) 102597.
[76] T. Wang, I. Can, S. Zhang, et al., ACS Appl. Mater. Interfaces. 10 (2018) 5835–5844.
[77] H.D. Yu, M.D. Regulacio, E. Ye, M.Y. Han, Chem. Soc. Rev. 42 (2013) 6006–6018.
[78] E. Yablonovitch, T.J. Gmitter, Phys. Rev. Lett. 63 (1989) 1950.
[79] P. Yao, G.J. Schneider, D.W. Prather, et al., Opt. Express. 13 (2025) 2370–2376.
[80] J.H. Moon, S. Yang, Chem. Rev. 110 (2010) 547–574.
[81] J. Xu, C. Fu, Q. Zhu, et al., ACS Nano 19 (2025) 26065–26074.
[82] W. Wang, M.O. Tade, Z. Shao, Chem. Soc. Rev. 44 (2015) 5371–5408.
[83] Q. Wang, C. Pornrungroj, S. Linley, E. Reisner, Nat. Energy 7 (2022) 13–24.
[84] Y. Zhao, L. Zhang, Y. Liu, et al., Langmuir 38 (2022) 8719–8732.
[85] L. Jiang, S. Zhou, J. Yang, et al., Adv. Funct. Mater. 32 (2022) 2108977.
[86] Y. Ding, C. Wang, H. Zhao, Matter. 8 (2025) 102408.
[87] Y. Ding, Z. Li, S. Zheng, et al., J. Environ. Manage 392 (2025) 126774.
[88] M. Yue, H. Lambert, E. Pahon, et al., Renew. Sustain. Energy Rev. 146 (2021) 111180.
[89] J. Jia, L.C. Seitz, J.D. Benck, et al., Nat. Commun. 7 (2016) 13237.
[90] H. Zhao, M. Wu, J. Liu, et al., Appl. Catal. B: Environ. 184 (2016) 182–190.
[91] T.L. Madanu, L. Chaabane, S.R. Mouchet, et al., J. Colloid. Interface Sci. 647 (2023) 233–245.
[92] S.K. Karuturi, L. Liu, L.T. Su, et al., Nanoscale 3 (2011) 4951–4954.
[93] B. Hatton, L. Mishchenko, S. Davis, et al., Proc. Natl. Acad. Sci. U. S. A. 107 (2010) 10354–10359.
[94] H. Zhao, Z. Hu, J. Liu, et al., Nano Energy 47 (2018) 266–274.
[95] H. Zhao, C.F. Li, Z.Y. Hu, et al., J. Colloid. Interface Sci. 604 (2021) 131–140.
[96] J. Low, J. Yu, M. Jaroniec, et al., Adv. Mater. 29 (2017) 1601694.
[97] H. Wang, L. Zhang, Z. Chen, et al., Chem. Soc. Rev. 43 (2021) 5234–5244.
[98] H. Yang, Mater. Res. Bull. 142 (2021) 111406.
[99] Z. Wang, Z. Lin, S. Shen, et al., Chin. J. Catal. 42 (2021) 710–730.
[100] J. Liu, Y.H. Guo, Z.Y. Hu, et al., CCS Chem. 5 (2023) 372–384.
[101] F.I. Woodward, Curr. Opin. Plant Biol. 5 (2002) 207–211.
[102] S. Manabe, R.J. Stouffer, J. Geophys. Res. 85 (1980) 5529–5554.
[103] G. Yang, Y. Kuwahara, K. Mori, et al., Nano Res. 16 (2023) 4515–4523.
[104] A.R. Reddy, G.K. Rasineni, A.S. Raghavendra, Curr. Sci. 46 (2020) 57.
[105] G. Yang, Y. Kuwahara, K. Mori, et al., J. Phys. Chem. C 125 (2021) 3961–3971.
[106] Y. Han, Z. Jia, W. Gong, et al., Chem. Eng. J. 500 (2024) 157636.
[107] M. Tao, Z. Jia, H. He, et al., J. Colloid. Interface Sci. 678 (2025) 45–56.
[108] Z.J. Wang, H. Song, H. Liu, et al., Angew. Chem. Int. Ed. 59 (2020) 8016–8035.
[109] J. Zhou, H. Liu, H. Wang, Chin. Chem. Lett. 34 (2023) 107420.
[110] A. George, B. Shen, M. Craven, et al., Renew. Sustain. Energy Rev. 135 (2021) 109702.
[111] P. Jiang, W.R. Liu, K. Wang, et al., CCS Chem. 7 (2025) 2149–2160.